MTLA 38 (2024) 102270

Contents lists available at ScienceDirect

Materialia

journal homepage: www.elsevier.com/locate/mtla

Full Length Article

Short and medium range order in the rapidly solidified metallic liquid Ta: Atomic packing, connection modes, and pressure effect

A. Houba [a,*], M. El Ayoubi [a], A. Samiri [a], A. Atila [b], A. Hasnaoui [a,*]

[a] LS2ME Laboratory, Polydisciplinary Faculty of Khouribga, Sultan Moulay Slimane University of Beni Mellal, B.P. 145, Khouribga 25000, Morocco
[b] Department of Material Science and Engineering, Saarland University, Saarbrücken 66123, Germany

ARTICLE INFO

Keywords:
Molecular dynamics
Monoatomic metallic glasses
High pressure
Connections mode
Medium-range order

ABSTRACT

In this study, molecular dynamics (*MD*) simulations were utilized to explore the Short and Medium-Range Order (*MRO*) in the rapidly solidified metallic liquid tantalum (*Ta*). Radial distribution function (*RDF*) and Voronoi tessellation analysis (*VTA*) techniques were employed to thoroughly explore the effect of pressure on the connectivity and structural properties at the Short-Range Order (*SRO*) and *MRO* levels. Our findings indicate that, at a quenching rate of 10^{13} K s^{-1}, glassy states are achieved at or below 20 GPa, while crystalline phases emerge at 25 GPa. *VTA* analysis indicates a significant alteration in the local structure of glassy *Ta* with increasing pressure. Specifically, the fraction of icosahedral-like clusters decreases while the fraction of crystal-like clusters rises notably.

Furthermore, we highlight that icosahedral-like clusters strongly tend to form 3-atom connection mode, while crystal-like clusters prefer 2-atom and 4-atom connection modes. Notably, icosahedral-like clusters are identified as the primary contributors to the emergence of the left sub-peak in the second peak of the *RDF*. In contrast, all cluster types contribute to the appearance of the right sub-peak.

1. Introduction

Following the successful formation of Au-Si metallic glass (*MG*) in 1960 [1], there has been an ongoing and determined effort to discover new types of *MGs* and unravel the underlying mechanisms responsible for the formation of their amorphous non-crystalline structures [2]. This persistent exploration is driven by the promising potential of *MGs* in advanced technological applications and by the relationship between their structure and properties [3–5]. Various structural models, including efficient cluster packing [6], quasi-equivalent cluster packing [7], and the global packing model [8], have been proposed in recent decades to explain the atomic arrangement within *MGs*. In these models, well-determined (usually icosahedral-like) clusters are linked by sharing common atoms, and this linkage establishes a bridge from short to medium-range order (*SRO* to *MRO*). These models collectively contribute to a deeper understanding of how *MRO* is efficiently achieved within *MGs*. However, due to the intricate and diverse nature of internal interactions within various alloy systems, the specific details of atomic packing in *MGs* remain subjects of rigorous debate. None of these models can provide a definitive and unequivocal explanation for the splitting of the second peak (*SSP*) observed in the radial distribution function (*RDF*). This splitting is widely recognized as a key indicator of the transition from a liquid state to a glassy state [9,10]. Recently, Liu et al. proposed that the overall atomic packing in *MGs* can be well explained as a mix of spherical-periodic order (*SPO*) and local translational symmetry (*LTS*) [8,11]. Significantly, they also suggested that the emergence of the *SSP* in the *RDF* is linked to the formation of *LTS* during the glass-forming process. Another contribution to this understanding comes from the work of Pan et al., who proposed that the irregular manner in which atomic clusters are connected leads to the observed *SSP* [12]. Specifically, they identified that the resulting two sub-peaks are attributed to a face-sharing (*FS*) connection and a vertex-sharing (*VS*) connection. In Zr-based *MGs*, it has been found that the *MRO* in these glasses is primarily governed by the formation of icosahedral clusters, which represent organized regions of atoms over short distances [13]. Other studies go further, combining experimental techniques with atomistic simulations. For example, Sheng et al. [7] explored atomic packing and short-to-medium range order in range of binary *MGs* through a combination of *XRD* and *EXAFS* experiments, along with ab initio calculations, molecular dynamics (*MD*), and reverse Monte Carlo simulation.

* Corresponding authors.
E-mail addresses: adil.houba@usms.ma (A. Houba), hasnaoui59@hotmail.com (A. Hasnaoui).

https://doi.org/10.1016/j.mtla.2024.102270
Received 10 June 2024; Accepted 18 October 2024
Available online 19 October 2024

Notably, numerous studies have attributed the origin of the *SSP* in *RDF* to the presence of icosahedral clusters [14–18]. Generally, both *MD* simulations and experimental measurements have consistently recognized icosahedral-like structures as the main building blocks in *MGs* [9,17,19,20]. However, the significance of the contribution of crystal-like and mixed-like clusters to the second peak in *RDF* is not as extensively studied. Consequently, a critical need exists for in-depth analysis of diverse clusters characterized by different Voronoi indices. This analysis is essential for understanding how these various clusters influence the second peak observed in *RDF* within the context of *MGs*. The prevailing understanding within the scientific community acknowledges that the *SSP* in the *RDF* is a consequence of how atomic clusters are interconnected [12,21,22]. Earlier studies [18,22–24] primarily focused on the analysis of decomposed components within *RDF* originating from various types of cluster connections. These connection types include *VS*, where a single atom connects two neighboring polyhedra; Edge Sharing (*ES*), where two neighboring polyhedrons share two atoms; *FS*, where two neighboring polyhedrons share three atoms; and finally, Squashed Tetrahedra Sharing (*STS*), involves connecting two neighboring polyhedrons with four atoms, nearly in the same plane but not strictly forming a perfect quadrangle face. However, difficulties arise when attempting to decompose the *RDF* in situations where the second peak does not manifest an evident split peak. This challenge hinders the ability to track the evolution of cluster connections throughout the cooling process.

Among the external parameters capable of influencing the glass formation in materials, pressure is a noteworthy factor. In the case of iron, it has been documented that an increase in pressure promotes the formation of crystalline clusters within the amorphous system [25]. Additionally, Jiang et al. [26] have noted that in monoatomic tantalum (*Ta*) *MGs*, the fraction of crystal-like clusters notably increase with increasing pressure, while the fraction of icosahedral-like clusters undergoes a noticeable decrease. It is crucial to emphasize that studies have demonstrated the substantial impact of pressure on the structure of *MG* [25–28]. However, the impact of pressure variation on the *MRO*, especially during the dynamic super-cooling process, continues to be not fully comprehended. Recent experiments [29,30] have successfully obtained monatomic MGs, which represent the simplest form of glass and offer a foundational framework for gaining insights into the interplay between the physical properties and structural aspects of *MGs*. Moreover, in the case of monatomic *MGs*, where factors such as element mixture effect and atomic size variation are absent, the core structural characteristics are naturally spotlighted. In the present study, molecular dynamics (*MD)* simulations were employed to investigate the effect of temperature and pressure on the short- and medium-range structure of a monoatomic *MG*, with the choice of *Ta* as the selected metal prototype. By simulating the process of glass formation under pressure through rapid cooling from a liquid state, a thorough examination was conducted to analyze the local atomic structures and their connections. The main objective of this study is to systematically examine these connection patterns as the system undergoes cooling under a broad range of pressures, primarily relying on Voronoi analysis.

2. Methodology

Using the Large-scale Atomic/Molecular Massively Parallel Simulator (*LAMMPS*) [31], a series of *MD* simulations were conducted to investigate the rapid solidification of *Ta* under varying pressures. Firstly, 250,000 atoms are arranged within a cubic box according to a body-centered cubic (*bcc*) structure with a lattice constant of 3.3 Å Periodic boundary conditions (*PBC*) are applied to mimic bulk properties. The Verlet algorithm is used to numerically solve Newton's equations of motion with a time step of 1 *fs*. The interatomic interaction was described by the embedded-atom method (*EAM*) potential, where the total energy depends on the electron density and atomic pair interactions:

$$E_{tot} = \sum_i F_i(\rho_{h,i}) + \frac{1}{2}\sum_{i \neq j} \varnothing_{ij}(r_{ij}) \quad (1)$$

Where $F_i(\rho_{h,i})$ denotes the embedding function of atom i within its atomic environment according to the total electron density $\rho_{h,i}$. The interaction between atom i and j is described by the function $\varnothing_{ij}(r_{ij})$ where r_{ij} represents the interatomic distance. In this study, we employed the parameterization of the *EAM* potential developed by Ravelo et al. [32]. Even though it was initially designed for crystals, this method has been found to be also suitable for amorphous structures as well [20,26,33–35]. For instance, the *RDF* of amorphous *Ta* predicted by this potential aligns closely with that obtained from ab initio simulations [33]. Additionally, under the *NPT* statistical ensemble (constant number of particles, pressure, and temperature), we heated the initial crystal from 300 K to 4000 K (the melting point from simulations is 3530 K) to ensure the liquid state was achieved, with pressure adjusted to zero. The pressure was then gradually increased over 1 ns to the desired value and held constant for 0.5 ns. Subsequently, under the *NPT* ensemble, the system was quenched to 300 K at a cooling rate of 10^{13} K s^{-1} under the same desired pressures (ranging from 0 to 25 GPa). The pressure was then released, and the system was relaxed for an additional 1 ns at 300 K. Atomic configurations of different samples were collected for the structural analysis. The *VTA* was utilized to examine the *SRO* of the structure. To determine the *MRO* feature of each sample configuration, we wrote a python code to compute the different scheme of connectivity between different *SRO* clusters. The analysis and visualization were conducted using OVITO (Open Visualization Tool) software [36].

3. Results and discussions

3.1. The short-range order

The volume of the system versus temperature is illustrated in Fig. 1, for different pressure values. The findings indicate that the glass transition temperature (*Tg*: defined as the temperature of the slope change) of *Ta* increases with an increase in pressure. This aligns well with the reported data for both iron [25] and hafnium [37] *MGs*. This is attributed to a reduction in atomic mobility and an increase of structural ordering under high-pressure conditions [27,28]. The *Tg* values for *Ta* were determined to be 1710 K, 1770 K, 1811 K, 1850 K, and 1900 K for

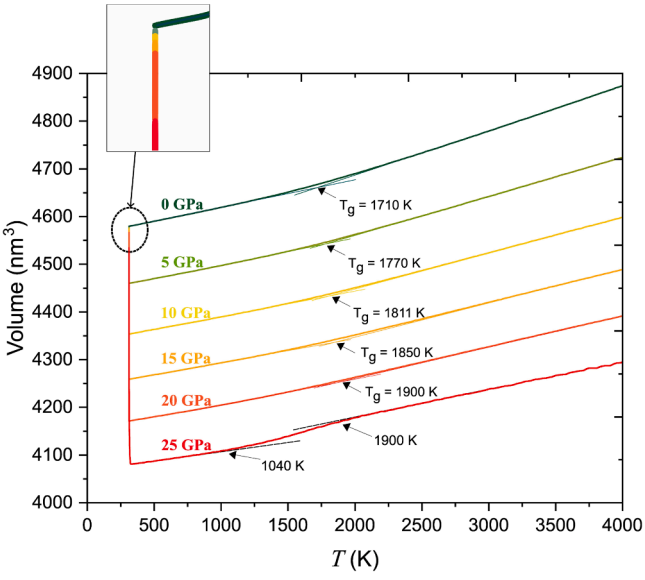

Fig. 1. Temperature-dependent variation of the volume of Ta at different pressures during rapid cooling.

pressures of 0, 5, 10, 15, and 20 GPa, respectively. Our result agrees well with that obtained by Jiang et al. [38] who studied the same system. Furthermore, our simulations revealed an absence of clear indication of crystallization up to 20 GPa, indicating that the system remained in a glassy state under these conditions. A subtle shift in the Volume-Temperature curves towards lower temperatures is observed at these pressures, indicating the transition from a liquid to a glassy structure. However, starting from 1900 K, a gradual decrease in volume was observed in sample quenched under 25 GPa, indicating that *Ta* had crystallized at this pressure. Thus, we estimate the critical pressure for *MG* formation at this cooling rate to be between 20 and 25 GPa. It is noteworthy that in both the liquid and solid state, the volume was lower for samples vitrified at higher pressures, likely due to the compressive effect of the increased pressure on the system's volume. After the pressure was released, the volume returned to a relatively similar value. However, in the sample quenched under 25 GPa, a lower volume was observed, as illustrated in the inset of Fig. 1. This reduction suggests that less free volume was present, further indicating that crystallization had occurred [39–41]. Overall, these findings imply that the structural evolution of *Ta* during rapid solidification is strongly influenced by the applied pressure.

We also conducted a structural investigation using *RDF* analysis, which describes the probability of locating an atom in a spherical shell with a radius r, and a center positioned on another atom. Its expression is given by [9,20,24]:

$$g(r) = \frac{V}{N^2}\left\langle \sum_{i=1}^{N} \frac{n(r)}{4\pi r^2 \Delta r} \right\rangle \quad (2)$$

Here, V represents the system volume, N indicates the total number of atoms, and n(r) denotes the number of atoms in the region situated between r and $r+\Delta r$. Fig. 2 depicts the *RDF* curves of *Ta* at 300 K after quenching under different pressures (0–25 GPa) and that of an ideal Ta crystal. When the applied pressure is <20 GPa, the resulting structures are amorphous, as evidenced by the split of the second *RDF* peaks [9,10]. However, when the system is cooled with a pressure of 20 GPa, a shoulder begins to form on the right side of the first maximum peak of the *RDF* curve. This suggests that the glassy structure is not fully stabilized and that there is an increase in the number of crystalline regions in the system. Moreover, our observations reveal that as pressure increases, there is a corresponding rise in the height of the first peak in the *RDF* curves, accompanied by a decrease in its width. This indicates that the *SRO* in the system is strengthening, and crystal nucleation continues to

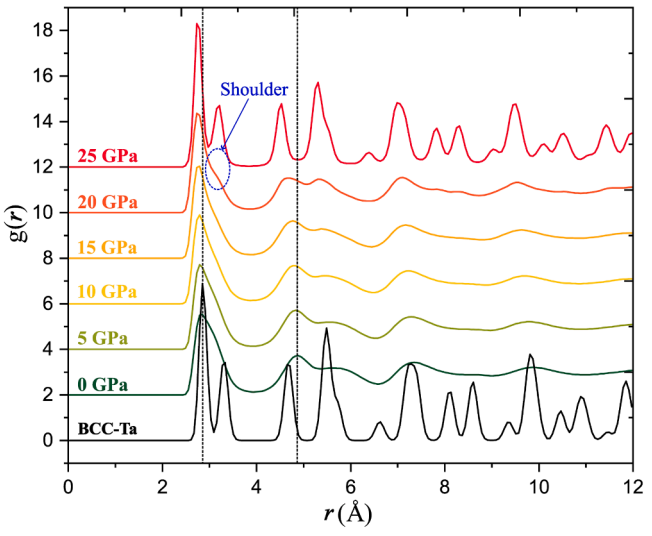

Fig. 2. Radial distribution function curves of Ta at 300 K after quenching under different pressures (0–25 GPa).

increase. Ultimately, a sharp crystalline phase with distinct *RDF* peaks is obtained at 25 GPa, which closely resembles the *RDF* of the *bcc* crystal structure, indicating the transformation to a *bcc* phase. Furthermore, our results demonstrate that an increase in pressure leads to a decrease in interatomic distances, reflected in the shift of the first and second peaks toward smaller values of *r*. This strongly implies that subjecting the system to higher pressure results in a more compact structural arrangement.

We also employed *VTA* to investigate the short-range structural differences of *Ta* models during the cooling process. This analysis allowed us to identify local atomic structures using the Voronoi indices $\langle n_3,n_4,n_5,n_6\rangle$, where n_i (i = 3,4,5,6) represents the number of i-edged faces in a Voronoi polyhedron (*VP*). For example, a perfect icosahedral has the Voronoi index ⟨0, 0, 12, 0⟩, indicating no faces with 3, 4, and 6 edges and 12 faces with five edges. As *MGs* don't have long-range order, they exhibit short and medium-range orders, which can be represented by Voronoi polyhedrons (*VPs*) and their arrangement into 3D networks. When constructing the Voronoi polyhedral, we deliberately excluded surfaces with an area <2 % of the total polyhedron surface area [7,42]. This approach was adopted to mitigate the problem associated with degeneracy and the potential influence of thermal vibrations. Following earlier studies [10,15], we grouped the *VP* types into three categories: Icosahedral-like clusters (including ⟨0,0,12,x⟩, ⟨0,1,10,x⟩, ⟨0,2,8,*x*⟩), mixed clusters (including ⟨0,3,6,x⟩, ⟨0,3,7,*x*⟩), and crystal-like clusters (including all ⟨0,4,4,x⟩ and bcc-like clusters such as ⟨0,6,0,8⟩) with x typically below 7. The "Icosahedral-like" structures include not only perfect icosahedral clusters ⟨0,0,12,0⟩, but also defective icosahedral ones such as ⟨0,1,10,2⟩ and ⟨0,2,8,4⟩, among others. Based on our previous analysis of *RDF*, a particular focus should be placed on bcc-like clusters. To this end, we employed adaptive common neighbors analysis (CNA), as used in OVITO, to identify atoms with bcc structures and track their respective Voronoi indices. Previous studies indicate that the *VP* index ⟨0,6,0,8⟩ is closer to representing an ideal bcc structure compared to any other *VP* types [25,41].

In the present study, we tracked the changes in the fractions of various *VPs* as the temperature decreased during the cooling process under varying levels of pressure, as depicted in Fig. 3*(a-e)*. Initially, the fractions of perfect icosahedral, defective icosahedral, mixed-like, and crystal-like clusters showed a pressure-independent behavior in the liquid phase. However, as the temperature decreased to the supercooled region (T < 2100 K), these fractions began to diverge, indicating that the applied pressure influenced their behavior. We observe that lowering the temperature during the transition from liquid to glass led to a more rapid increase in the fraction of perfect icosahedral clusters, along with a similar trend for distorted icosahedral clusters in systems quenched under pressures up to 20 GPa. However, this behavior tends to be inverted when pressure increases beyond 20 GPa, where the number of icosahedral-like clusters decreases as temperature decreases towards 300 K. These findings show that *Ta MGs* quenched under lower pressure (<20 GPa) have a better glass−forming ability, which is consistent with previous simulations results [25,37,38]. Fig. 3*(f)* illustrate the dominant types of *VPs* in the system under pressures ranging from 0 to 20 GPa at 300 K. The fraction of each *VP* varies with pressure, indicating changes in the local atomic structures across the systems under different pressures, even though they all exhibit an amorphous-like *RDF* pattern. It can be clearly seen that the fraction of ⟨0,0,12,0⟩ and distorted icosahedral *VPs* decreases with increasing pressure, while the fraction of ⟨0,6,0,8⟩ and ⟨0,4,4,6⟩ *VPs* increases. This indicates a structural transition from a more amorphous-like structure to a more crystal-like structure in the system. While both decreasing temperature and increasing pressure led to the densification of the metallic liquid, they exert distinct influences on the local atomic structures. Pressure alters the atomic environment around individual atoms within the liquid, which, in turn, affects the creation and stability of icosahedral-like clusters. Under higher pressures, the atomic arrangements tend to favor the formation of crystal-like clusters over icosahedral-like ones. When pressure increases,

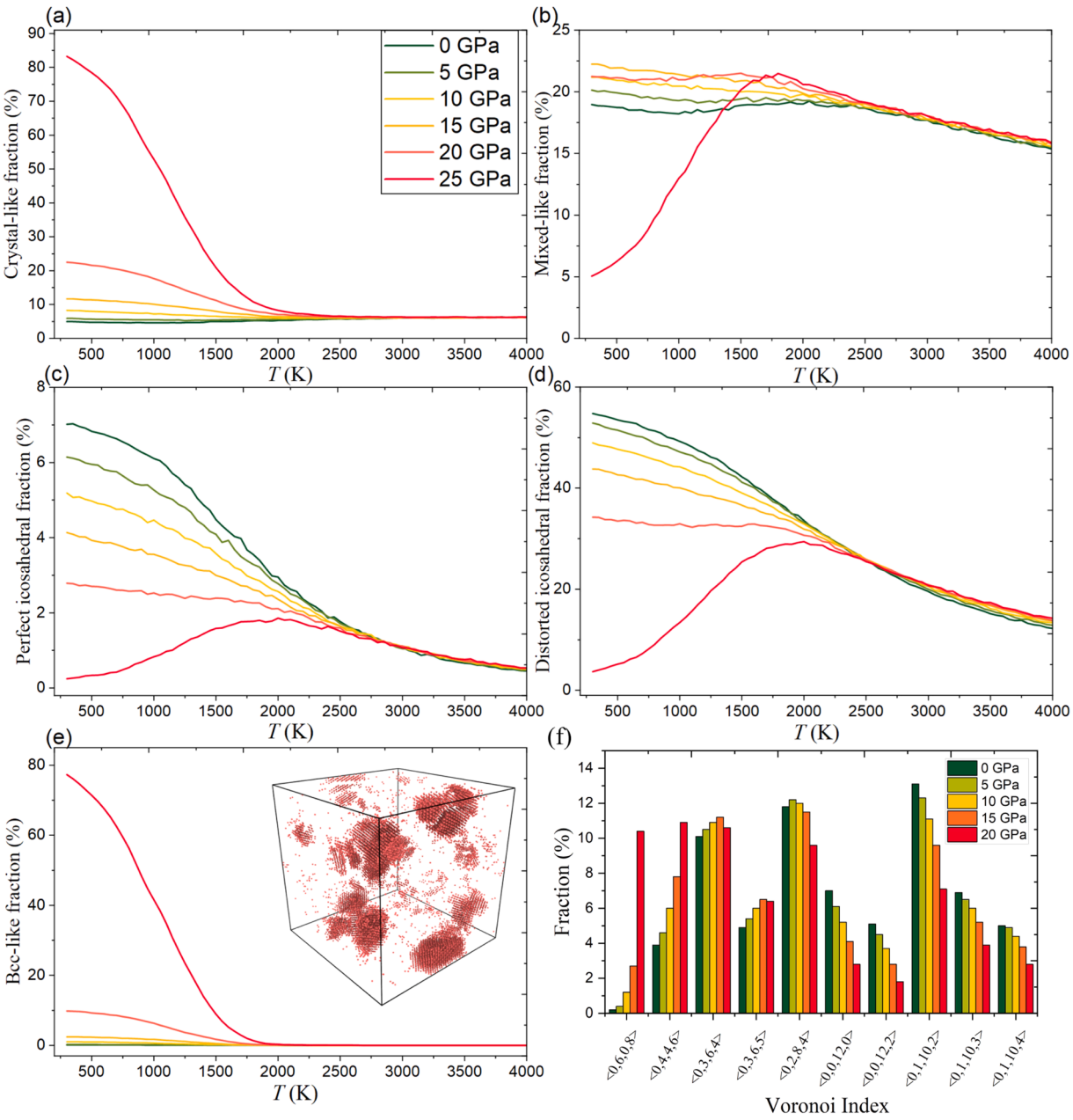

Fig. 3. Temperature evolution of fraction of the (a) crystal-like, (b) mixed-like, (c) perfect icosahedral, (d) distorted icosahedral and (e) bcc-like clusters for various pressures. The inset shows the distribution of bcc-like cluster at 20 GPa (f) Pressure dependence of dominated Voronoi polyhedrons in Ta at 300 K.

crystal structures, being tightly packed, are more likely to be formed than disordered amorphous structures [25], and it is widely accepted that *VPs* with small Local fivefold symmetry ($n_5 \leq 4$), have a stable crystalline structure [43], while *VPs* with high Local fivefold symmetry ($n_5 \geq 8$), has a metastable amorphous structure [20,27]. Which explains the significant increases in crystal-like clusters, reaching 23 % and 83 % for samples quenched under 20 GPa and 25 GPa, respectively. Furthermore, the observed increase in the fraction of bcc-like clusters at 300 K from 0 % at 0 GPa to 2.4 %, 9.9 %, and 77 % for samples quenched under 15 GPa, 20 GPa, and 25 GPa, respectively, indicates the presence of crystalline regions that are randomly distributed within the amorphous matrix. This is illustrated in the inset of Fig. 3*(e)*. Overall, the increased pressure leads to densification of the Ta metallic liquid, which can increase the likelihood of crystal nucleation and growth and reduce the amount of time available for icosahedral-like clusters to form. This is confirmed by the *RDF* observations, which indicate that higher pressure promotes the formation of bcc orders rather than icosahedral orders in the rapidly solidified *Ta*.

3.2. The medium-range order

To investigate the atomic packing feature beyond the short-range length scales, we analyzed the connection of atomic clusters. This approach provides insights into the connectivity of atomic clusters and can be determined by computing the number of shared neighbor atoms between each pair of clusters. In Fig. 4*(a)*, the *MRO* network is depicted, consisting of perfect icosahedral clusters and bcc-like clusters present in a *Ta* model quenched under 25 GPa at 1700 K. The atoms are color-coded based on the type of polyhedron, with red indicating perfect icosahedral clusters and orange representing bcc-like clusters, as shown in Fig. 4*(b)*. Furthermore, the neighboring *SRO* packing can be categorized into four types, as elucidated by the insert snapshots in Fig. 4*(c)*.

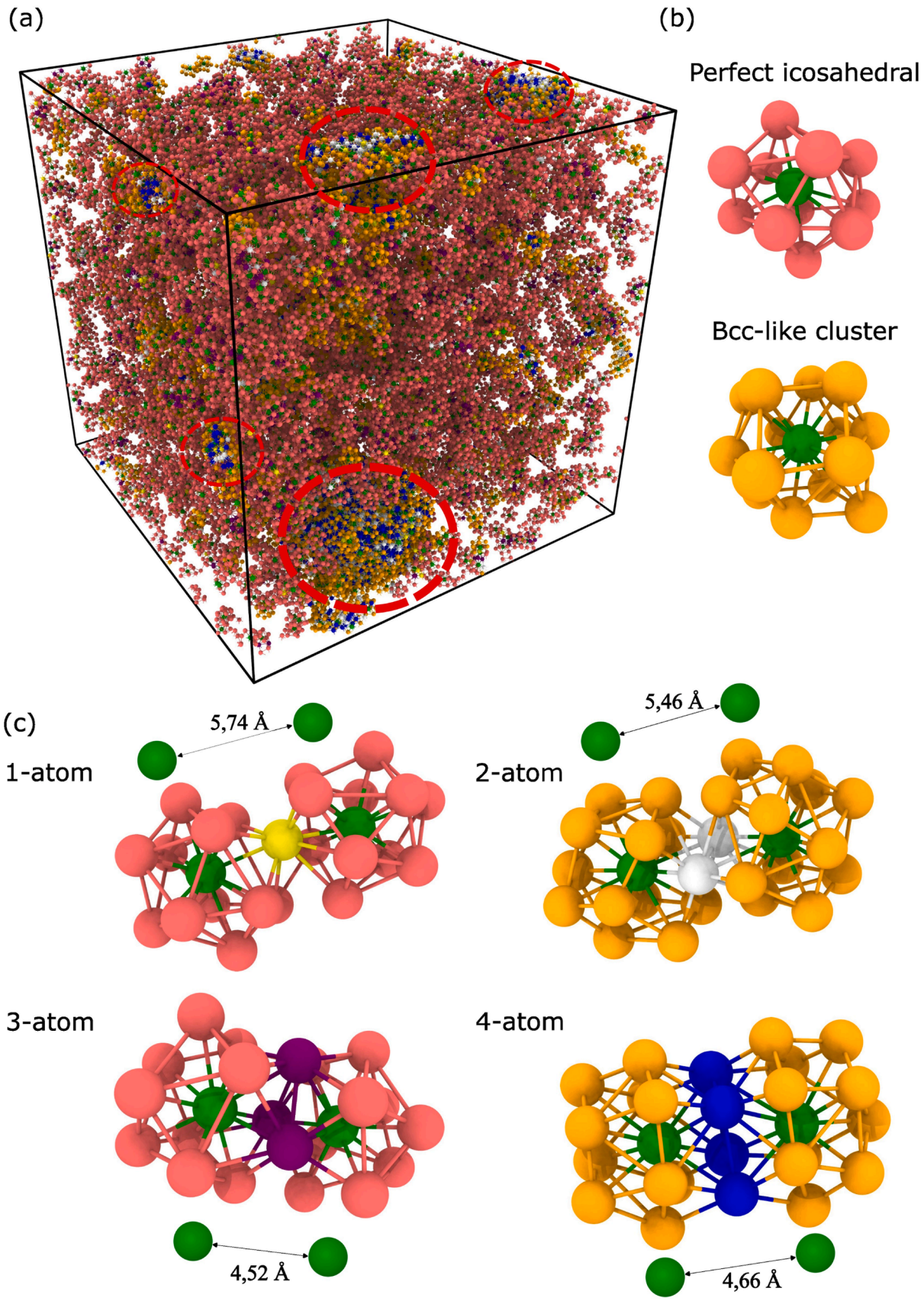

Fig. 4. (a) snapshot depicting perfect icosahedral and bcc-like cluster configuration in Ta sample quenched under 25 GPa at 1700 K (b) perfect icosahedral and bcc-like cluster (c) Illustrations of 1-, 2-, 3-, and 4- atom connection modes. The green, yellow, white, purple and blue atoms represent the central, 1-, 2-, 3-, and 4- atom, respectively.

These clusters can share one, two, three, or four atoms, where the connecting atoms are color-coded as yellow, white, purple, and blue for 1-, 2-, 3-, and 4-atom connection schemes, as shown in Fig. 4*(c)*, respectively [9,21,44]. The average distances between the central atoms of the two icosahedral clusters connected by 1- and 3-atom connections are 5.74 Å and 4.52 Å, respectively, as shown in Fig. 4*(c)*. Similarly, the average distances between the central atoms of the two bcc-like clusters connected by 2- and 4-atom connections are 5.46 Å and 4.66 Å, respectively. Additionally, As illustrated in Fig. 4*(a)*, the crystalline regions, identified as regions enclosed by red dashed circles, correspond to bcc-like clusters characterized mostly by the Voronoi index ⟨0,6,0,8⟩. Within these regions, a significant proportion of atoms are color-coded in white and blue. Hinting at a preference for 2-atom and 4-atom connection schemes. In contrast, for perfect icosahedral clusters, there appears to be a preference for a 3-atom connection scheme. Fig. 5 illustrates the evolution of cluster connections with decreasing temperature for samples quenched under different pressures (0–25 GPa). The results show that at 0 GPa, the fraction of 3-atom connections exhibited a substantial increase with decreasing temperature while the fraction of 1-atom, 2-atom, and 4-atom connection modes showed a decrease. An investigation by Ding et al. established that slower cooling rates lead to an increase in structural ordering. This is associated with a decrease in 2-atom and 4-atom connection modes and an increase in the number of 3-atom connections [23]. Furthermore, since the total number of connections increases slightly during the quenching process, we report in Table 1 the change in count (%) for each of the four cluster connection modes between the liquid and solidified states. A positive percentage indicates an increase, while a negative percentage indicates a decrease compared to the liquid state. For example, a percentage of 100 % means the count of the connection mode has doubled compared to the liquid state. From this table, we see that for the sample at 0 GPa, the count of

Table 1
The change in count (%) for each of the four cluster connection schemes between the liquid temperature $T = 4000$k and $T = 300$ K of Ta formed using different pressures.

	0 GPa	5 GPa	10 GPa	15 GPa	20 GPa	25 GPa
1-atom (%)	−0.30	−0.68	−1.42	−2.55	−5.77	−26.67
2-atom (%)	−19.59	−17.11	−13.17	−8.09	4.23	69.58
3-atom (%)	63.29	57.22	49.10	39.30	19.33	−74.39
4-atom (%)	−2.63	2.12	11.10	22.69	59.17	315.23

the 1-atom mode remains almost unchanged. Essentially, this implies that the increase in the count of 3-atom connections comes at the expense of the 2-atom and 4-atom connection modes. Additionally, as the temperature continues to decrease, more icosahedra link with each other, potentially resulting in the emergence of new 3-atom connection modes [45]. In contrast, with increasing pressure, the fraction of 2-atom and 4-atom connection modes increases, while the fraction of 1-atom and 3-atom connection modes decreases. This trend increasingly pronounced as the pressure increased. It indicates that increasing pressure leads to a shift in the atomic packing structure from icosahedral-like to more crystal-like arrangements. This shift involves the formation of clusters that share more common neighbor atoms that are spaced closer together, forming a bcc structure. Interestingly, among *Ta* samples studied in this work (0–20 GPa), 1-atom and 4-atom connection modes were found to have the highest and lowest fractions, respectively. This pattern has been observed in many previous studies on *MGs* [12,24]. However, the *Ta* sample cooled under 25 GPa, which underwent crystallization, exhibited the highest fraction of 2-atom and the lowest fraction of 3-atom connection modes. These findings suggest that the formation of specific types of connections is strongly influenced by the

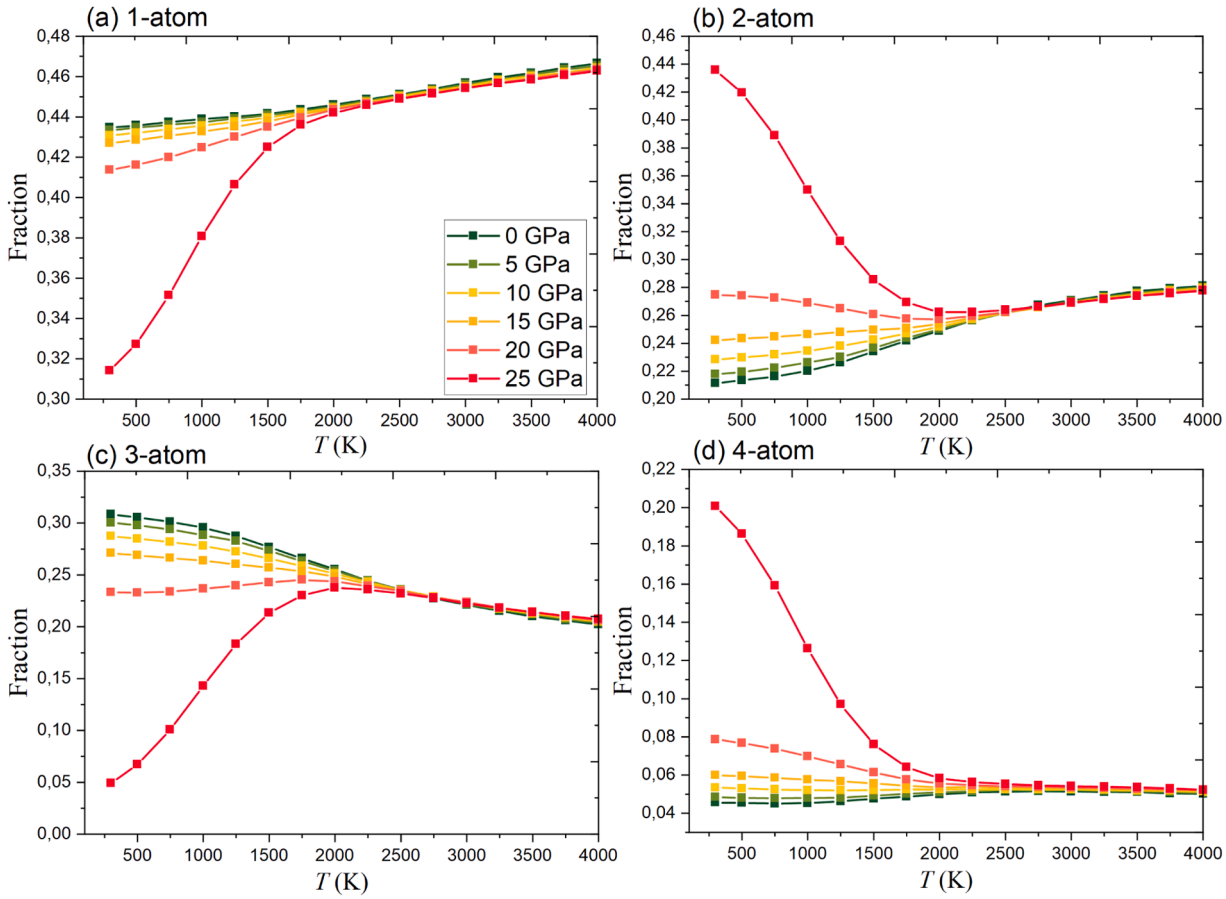

Fig. 5. Evolution of fraction of (a) 1-atom (b) 2-atom, (c) 3-atom and (d) 4-atom connection with decreasing temperature for various pressures.

structural state of the material, which can be tuned by external factors such as pressure, and that the splitting of the second peak in the *RDF* for *MGs* is due to different cluster connection modes compared to the liquid and crystal states.

As shown in Fig. 6 we conducted further investigations to explore the preferred type of connections between different groups of clusters, including perfect icosahedral, distorted icosahedral, mixed-like, and crystal-like clusters of Ta at 300 K after quenching and releasing pressure. The connection preferences between different groups of clusters were found to be distinct. For instance, icosahedral-like structure, including perfect icosahedral and distorted icosahedral clusters, exhibited a strong tendency to form 3-atom and 1-atom connection mode among themselves and with other cluster groups, as illustrated by the red, black and green curves in Fig. 6*(a,c)*. Additionally, they displayed a low fraction of 2-atom and 4-atom connection modes (see Fig. 6 *(b,d)*), which is consistent with the findings of Mirim et al. [46]. Their study revealed that out of the four different icosahedral linking patterns, the 2-atom connection mode was found to have the lowest fraction in both $Cu_{50}Zr_{50}$ and $Cu_{65}Zr_{35}$ compositions. In contrast, crystal-like clusters demonstrated a strong inclination to form 2-atom and 4-atom connection. This tendency increases with rising pressure, especially for "crystal-like - crystal-like" connected clusters, this increase can be attributed to the emergence of bcc-like clusters at high pressures, which exhibit a greater tendency to form 2-atom and 4-atom connections compared to other crystal-like clusters, as shown by the brown curve in Fig. 6*(b)* and Fig. 6*(d)*. This is likely due to the unique structural characteristics of the ideal *bcc* cluster, featuring six quadrangle and eight hexagonal faces. For mixed-like clusters, their connection tendencies vary depending on the clusters they connect with. When connecting with icosahedral-like clusters, they exhibit a strong preference for 1-atom and 3-atom connections. However, when establishing connections with crystal-like clusters, they tend to form 2-atom and 4-atom connection modes. Lastly, when connecting with other mixed-like clusters, their tendency to form all types of connections is relatively balanced compared to other clusters connections present in the system. In our observations, we have found that both pressure and the local atomic arrangement have minimal influence on the connection preferences of different cluster groups, especially in *MGs* (systems quenched at 20 GPa or lower). This is particularly evident when examining the behavior of "bcc-like – bcc-like" connected clusters. Even at 20 GPa, where the structure begins to crystallize, there is no significant change in the tendency to form 2-atom and 4-atom connections. Other clusters show limited response to structural changes. For example, when icosahedral-like clusters are involved, the 1-atom connection mode decreases with increasing pressure. This observation is particularly highlighted in the 25 GPa sample. In the investigation conducted by Pan et al. [12], it was ascertained that the emergence of two distinct sub-peaks could be attributed to a 3-atom connection and a 1-atom connection mode, respectively. When analyzing Fig. 6*(c)*, it becomes evident that "perfect icosahedral – distorted icosahedral" connected clusters exhibit the highest tendency to form the 3-connection mode, followed by "perfect icosahedral – perfect icosahedral" and "distorted

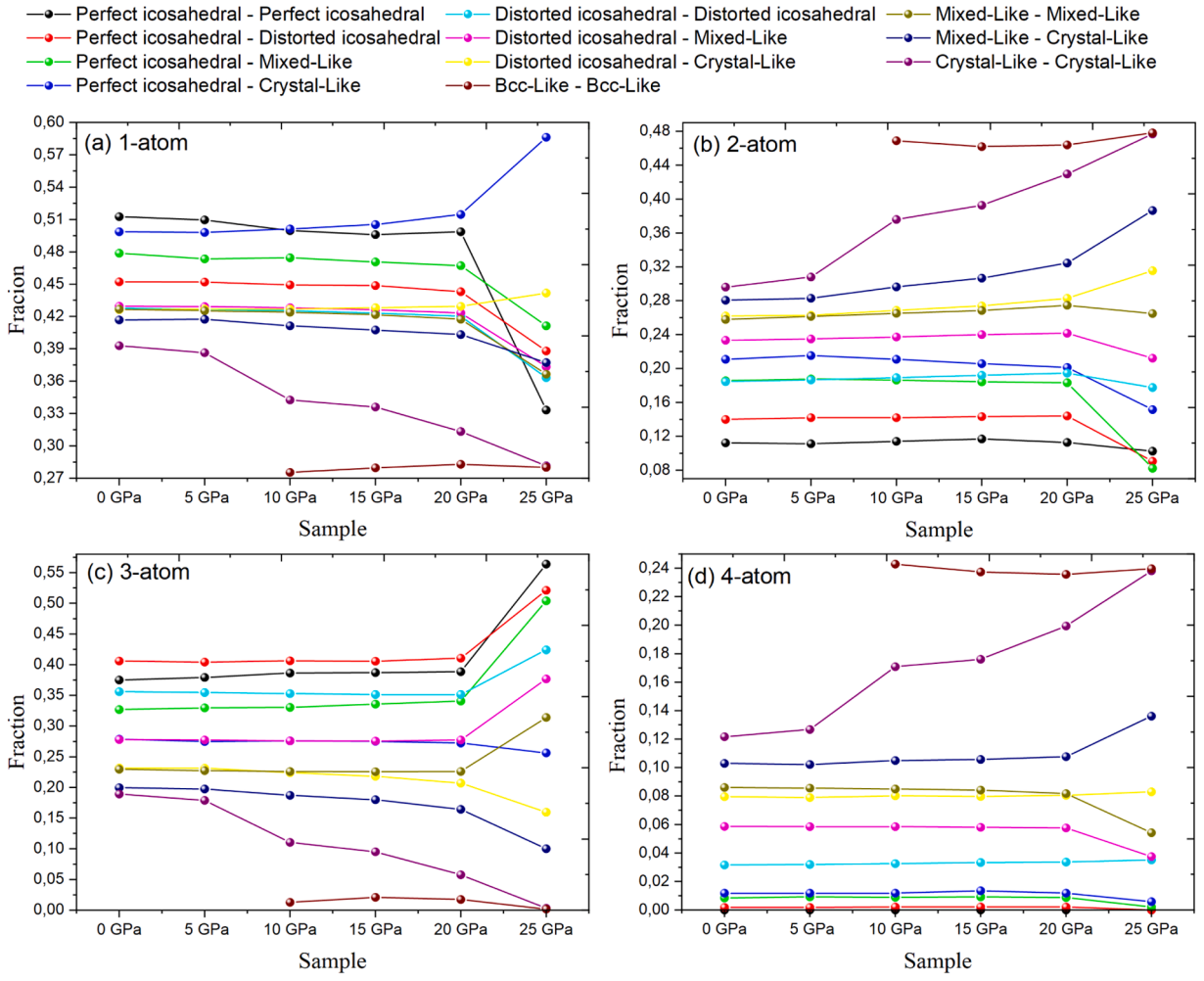

Fig. 6. Evolution of fraction of (a) 1-atom, (b) 2-atom, (c) 3-atom, and (d) 4-atom connections with increasing pressure at 300 K, Classified by different cluster groups.

icosahedral – distorted icosahedral" connected clusters. This underscores the significant role of icosahedral-like clusters in the emergence of the left sub-peak. Regarding the 1-atom connection mode, "perfect icosahedral – perfect icosahedral" connected clusters show the strongest tendency to form this type of connection, followed by "perfect icosahedral – crystal-like", "perfect icosahedral – mixed-like" and "perfect icosahedral – distorted icosahedral" connected clusters. Surprisingly, all clusters in the system contribute significantly to the appearance of the right sub-peak with, perfect icosahedral clusters being the major contributors. It is important to highlight that some specific modes of connections are absent within certain cluster groups or nearly non-existent. For instance, the 3-atom connection mode is almost non-existent for "bcc-like – bcc-like" connected clusters, with a fraction close to 0, aligning with the observations made by Pan et al. [12]. Their research indicates that in an ideal *bcc* Fe crystal, clusters are typically connected by 4, 2, or 1 common atoms, while the 3-atom connection mode is absent. Additionally, another example is the absence of the 4-atom connection mode in "perfect icosahedral – perfect icosahedral" connected clusters in all the systems of Ta we examined. Therefore, this connection mode cannot occur.

To comprehend the varying tendencies of cluster groups to form specific connections, we initiated our investigation by calculating the average thermal energy for each specific cluster involved in each specific connection mode. Considering all the atoms within these clusters, this energy includes the sum of kinetic and potential energies for clusters engaged in 1-atom, 2-atom, 3-atom, and 4-atom connection modes. This analysis was carried out for systems quenched under various pressures (0, 5, 10, 15, 20, and 25 GPa) at 300 K after releasing the pressure and letting the structure relax for 1 ns. The computed thermal energy values are averaged on all atoms involved in the considered connection mode. By doing so, we acquired a representative and comprehensive assessment of the thermal energy associated with each connection mode. Furthermore, we computed the average thermal energy for three specific connected clusters present in the system: "perfect icosahedral – perfect icosahedral", "crystal-like – crystal-like," and finally, "bcc-like – bcc-like". The results of these calculations are presented in Fig. 7*(a-d)*. In the case of connections involving the entire clusters within the system (see Fig. 7*(a)*), it becomes evident that in systems quenched at 10 GPa and below, the 3-atom connection mode exhibits the lowest energy. Our findings are in fair agreement with those found by El Ayoubi et al. [24] in their study of investigating the impact of cooling rate on *MRO* in Mg-Al *MGs*. They observed that the pair potential energy of the 3-connection mode exhibited the lowest atomic energy value in Mg-Al *MGs* for all five cooling rates they considered. The fact that the 3-atom connections have lower energy suggests they play a crucial role in stabilizing and forming the *MGs* structure. This implies that these 3-atom connections involve stronger bonding interactions compared to other connection modes. However, in systems quenched at a pressure of 15 GPa or higher, the 4-atom connection mode exhibited the lowest energy. This shift in energy levels implies a transformation from a glassy state to a more crystalline structure. When the system is quenched at 25 GPa, a notable and sudden decrease in the energy value of all connection modes was observed, due to the formation of a predominantly *bcc* crystalline structure. Importantly, the disparity in energy levels grew, making the 4-atom and 2-connection modes by far the most preferred, while the 3-connection mode became the least favored. Specifically, considering only the "perfect icosahedral – perfect icosahedral" connected cluster, as depicted in Fig. 7*(b)*, the 3-atom connection mode consistently had the lowest energy in all systems. However, in the system quenched at 25 GPa, where crystallization occurred, there was an increase in energy for

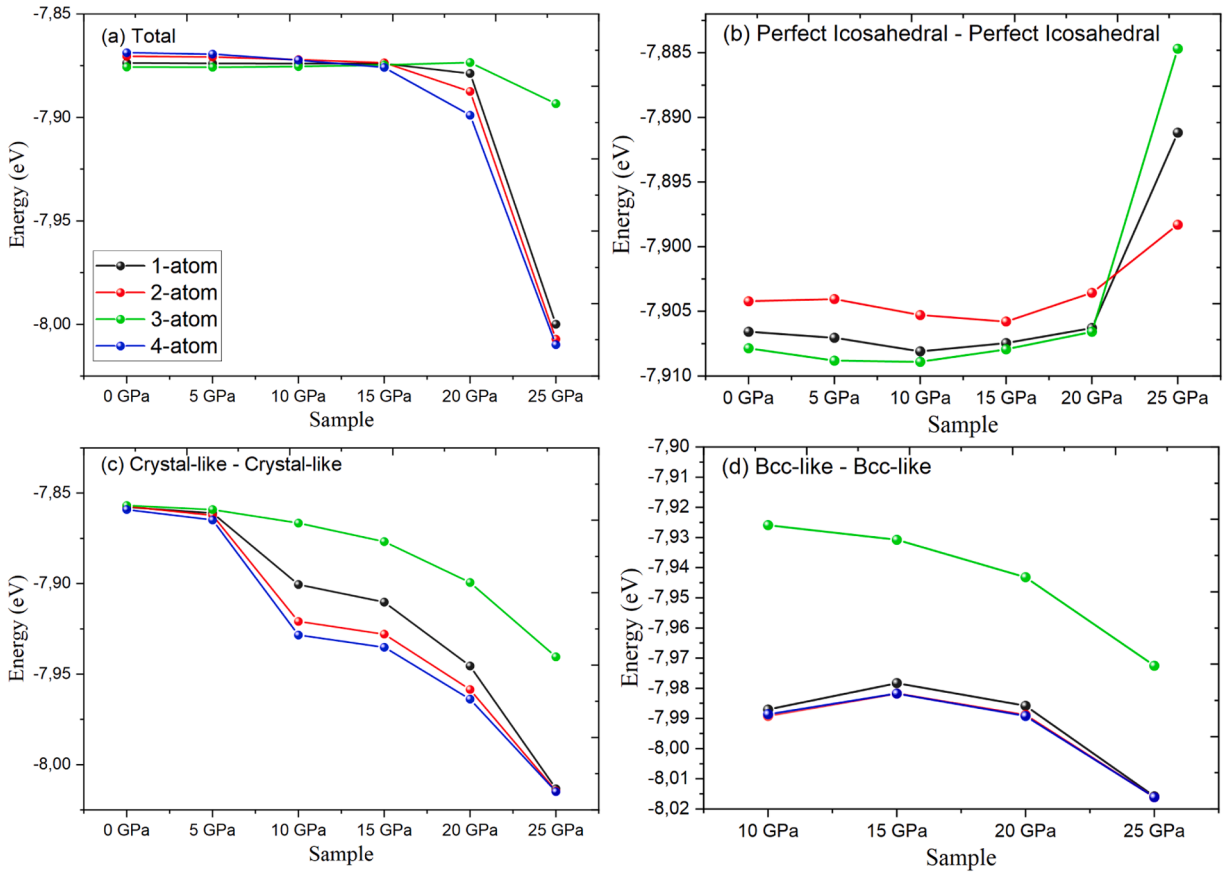

Fig. 7. Evolution of average energy in clusters involved in 1-atom, 2-atom, 3-atom, and 4-atom connections, respectively, with increasing pressure at 300 K, classified by different cluster groups.

all connection modes, indicating the instability of these perfect icosahedral clusters. Whereas, for the "bcc-like – bcc-like" connected clusters (see Fig. 7*(d)*), the 3-atom connection mode consistently exhibited the highest energy in all systems. Furthermore, as the pressure increased, the energy levels for the different connection modes decreased, suggesting an increase in stability. When considering other crystal-like clusters, including bcc-like clusters as depicted in Fig. 7*(c)*, we observed minimal differences in energy among various connection modes, with the 4-atom connection mode having the lowest energy in the sample quenched under 0 GPa. However, with increasing pressure, we observed a widening gap in energy between the 3-atom connection mode and the other connection modes. This trend is likely due to the increased prevalence of bcc-like cluster in samples quenched at higher pressures.

3.3. Second peak splitting

In this study, we also investigated the impact of different connection schemes on the second peak of the *RDF* in *Ta MGs*. Fig. 4(c) displays the four connection schemes we considered, each resulting in a distinct most-probable distance between the two *SRO* cluster centers. Consequently, the *RDF* exhibits peaks at different correlation distances for each connection scheme. The broad second peak in the *RDF* of *MGs* arises due to the superimposition of contributions from these four connection schemes. To explain the *SSP* in the *RDF*, which is not observed in liquids, we computed the average distances for 1-atom (Vs), 2-atom (Es), 3-atom (Fs_3), and 4-atom (Fs_4) connections for MGs at 300 K, following pressure release. Our results indicate that the average distances for 1-atom, 2-atom, 3-atom, and 4-atom connections mode are 5.97, 5.36, 4.86, and 4.28 Å, respectively, at 0 GPa, while at 20 GPa, we obtained values of 5.97, 5.36, 4.85, and 4.40 Å, respectively, for these connection types. In Fig. 8, we present the *RDF* obtained at 300 K for the system quenched under 0 GPa (see Fig. 8(a)) and 20 GPa (see Fig. 8(b)), to aid in visualization, we gathered all the distances between clusters in our system and created histograms that depict the number of data points within specific distance ranges for these connection schemes. In our case, we specified these distance bins to be 0.1 Å Regarding the sample quenched under 0 GPa, our observations reveal that the left sub-peak, illustrated in Fig. 8(a) at $R_1 = 4.86$ Å, is primarily associated with 3-atom connection mode. However, it is also somewhat affected by both 4-atom and 2-atom connection modes. On the other hand, the right sub-peak at $R_2 = 5.97$ Å is predominantly related to 1-atom connections but is still marginally influenced by 2-atom connections. For the system previously quenched under 20 GPa, a new peak emerges near $d_{ES} = 5.36$ Å, while the right sub-peak becomes no longer visible. This is likely due to the higher prevalence of 2-atom connections, which are more abundant at this pressure, while 1-atom connections associated with the right sub-peak are less frequent. The frequency of different types of atomic connections within a *MG* can provide insight into its glass forming ability (GFA) and potential for crystallization. Specifically, an increase in the frequency of 3-atom connections can promote glass formation, while a decrease in 1 and 3 atom connection modes and an increase in 2-atom connections can indicate the beginning of crystallization. These trends can be observed in the *RDF* presented in Fig. 8*(b)*, where the emergence of a new peak close to the average distance of 2-atom connection mode suggest the beginning of crystallization. This is further supported by the previous observation that show a higher percentage of crystal-like clusters and a lower percentage of icosahedral-like clusters in the metallic glass at 20 GPa. In fact, our previous results have shown that perfect icosahedral clusters have a very high tendency to form 3-atom and 1-atom connection modes compared to any other cluster group. Thus, the observed *SSP* of the *RDF* at 0 GPa can be attributed to the emergence of icosahedral-like clusters, which have a significant impact on the atomic connectivity and potential for vitrification.

In addition, we computed the partial *RDFs* for different cluster groups to investigate their influence on the emergence of the second *RDF* peak in the *Ta MGs* quenched under 0 GPa and 20 GPa respectively. The calculated partial *RDFs* for central atoms of crystal-like ($g_{crystal\text{-}like}(r)$), mixed-like ($g_{mixed\text{-}like}(r)$), perfect icosahedral ($g_{perfect\ icosahedral}(r)$), distorted icosahedral ($g_{distorted\ icosahedral}(r)$), and bcc-like ($g_{bcc\text{-}like}(r)$) clusters are depicted in Figs. 9*(a-d)* and 10*(a-e)*. Moreover, using the binning technique, we generated histograms with 0.1 Å intervals to illustrate counts per distance bin for different connection schemes. Generally, we observe that the more significant the difference between the counts of 2-atom connections with 1 and 3, the more pronounced the *SSP*. Moreover, the shaping for Partial *RDF* of icosahedral-like and mixed-like clusters did not change with pressure (see Figs. 9*(b-d)* and 10 *(b-d)*). Additionally, the shapes of $g_{distorted\ icosahedral}(r)$ closely resemble the second peak of Ta *MGs*, emphasizing their significant role in the formation of *MGs*. For perfect icosahedral clusters, the peaks are distinctly separated, a characteristic attributed to the lower abundance of the 2-connection mode, as seen in the blue histogram (see Figs. 9*(c)* and 10*(c)*). Similar findings have been reported in Ni [9] and Ni_3Al [21] *MGs*. While the splitting is still noticeable in the partial *RDF* curve of Mixed-like clusters. However, due to the lower count of the 3-atom connection mode and higher count of the 2-atom connection mode, the intensity of the left sub-peak is reduced. The partial *RDF* curve of crystal-like for unpressured sample shows the typical observed right sub-peak disappearing and new one emerging as shown in Fig. 9*(a)*. This change is due to the high abundance of 2-atom connection mode. On the other hand, the partial *RDF* curve of crystal-like clusters in the sample

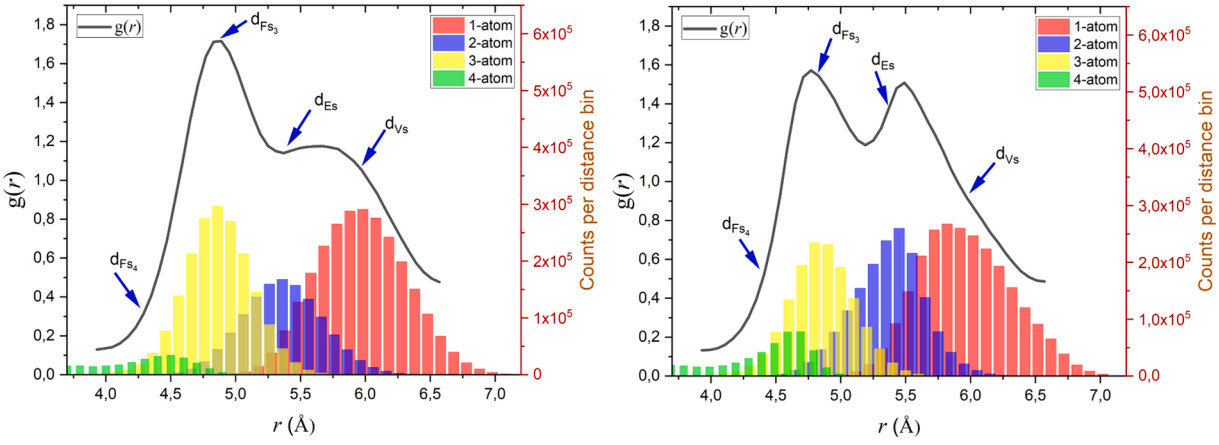

Fig. 8. Radial distribution functions for Ta at 300 K after quenching under a) 0 GPa and b) 20 GPa, displaying average distances for each connection mode with arrows.

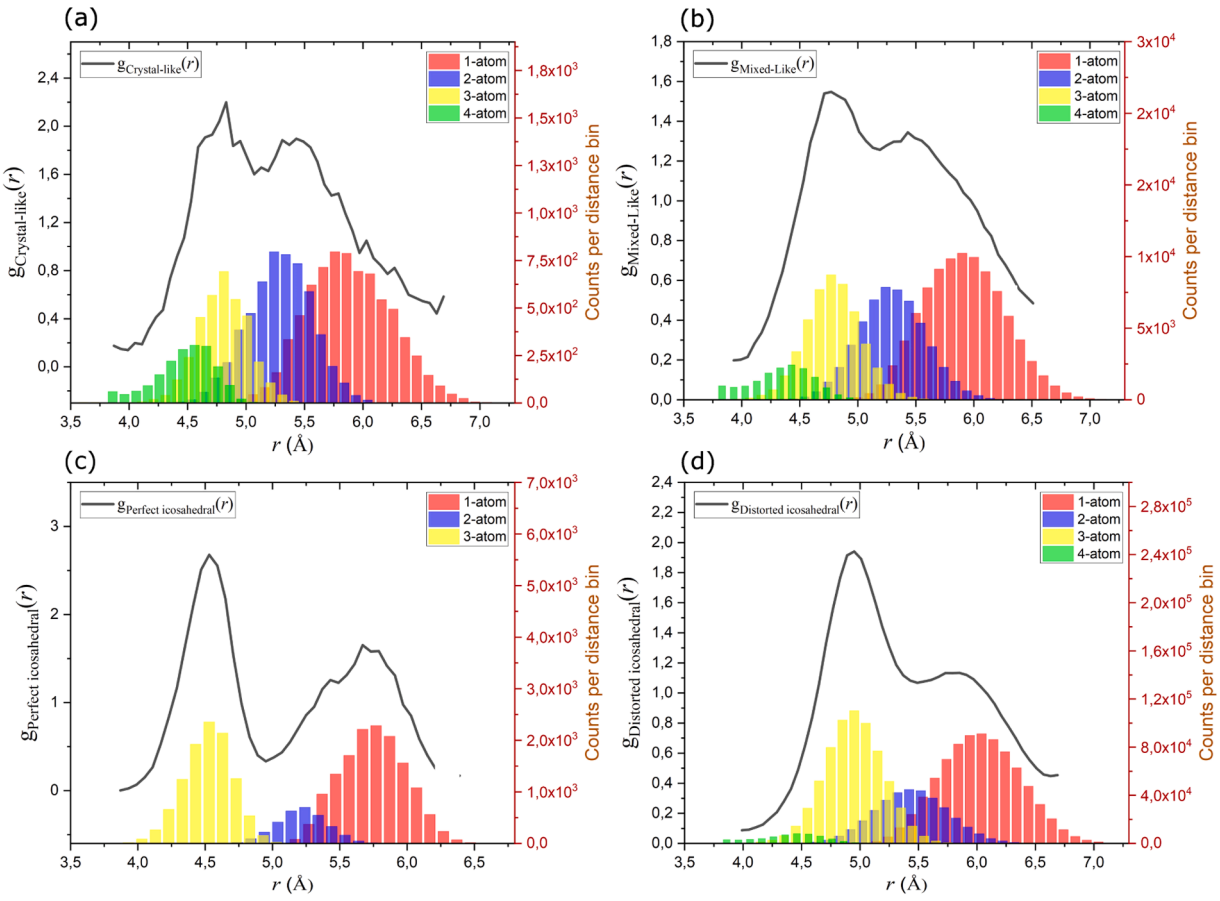

Fig. 9. Partial RDF curves of central atoms of (a) crystal-like, (b) mixed-like, (c) perfect icosahedral and (d) distorted icosahedral clusters in Ta at 300 K after quenching under 0 GPa.

quenched under 20 GPa contains three distinct peaks (left-, middle- and right-peak) resembling the *RDF* of a *bcc* structure (see Fig. 10*(a)*). The left-peak is primarily formed by the 4-atom connection mode with a minor contribution from the 3-atom connection mode. The middle-peak is mainly shaped by the 2-atom connection mode with some contribution from the 1-atom connection mode. The subtle right-peak is formed only by the 1-atom connection mode. The partial *RDF* of bcc-like clusters closely resembles $g_{crystal\text{-}like}(r)$, with the exception that the peaks are narrower and more intense, indicating a higher degree of order. Interestingly, the left-peak lacks contribution from the 3-atom connection and is primarily formed by the 4-atom connection mode. This further demonstrates that the emergence of bcc-like clusters is the primary reason for the disappearance of the right sub-peak and the emergence of a new peak, as illustrated in Fig. 8*(b)*.

4. Conclusion

To summarize, the current investigation examined the atomic packing characteristics of rapidly solidified Ta and studied their behavior under pressure. It is found that at pressures up to 20 GPa, quenching at 10^{13} K s^{-1} leads to the formation of amorphous structures, as indicated by the *SSP* in the *RDF*. The increase of pressure favors the formation of crystal-like clusters in the amorphous systems. We analyzed the connection of atomic clusters on the *MRO* level based on *VTA*. The results indicate that the structural state of the material and external factors, such as pressure, considerably affect the formation of types of connections. An increase in pressure led to a shift in the atomic packing structure from icosahedral-like to more crystal-like arrangements, resulting in the formation of clusters that displayed higher fractions of 2-atom and 4-atom connection modes. The *RDF* exhibited distinct peaks at different correlation distances for each connection scheme, which resulted in a broader second peak of the *RDF* in *MGs* due to the overlapping contributions from these connection schemes. To explain the observed *SSP* in the *RDF*, the average distances for various types of connections at 0 GPa and 20 GPa were computed. The results revealed that an increase in the frequency of 3-atom connections can enhance the glass formation process, whereas a decrease in 1 and 3-atom connections and an increase in 2-atom connections can signify the onset of crystallization. This finding was further supported by the emergence of a new peak near the most probable distance of 2-atom connections in the *RDF* at 20 GPa, indicating the beginning of crystallization. Therefore, the *SSP* in the *RDF* at 0 GPa is due to the presence of icosahedral-like clusters, which tend to form 3-atom and 1-atom connection modes. Our findings highlight that icosahedral-like clusters play a key role in the emergence of the left sub-peak of the second *RDF* peak, while all cluster types contribute to the right sub-peak.

CRediT authorship contribution statement

A. Houba: Writing – original draft, Writing – review & editing, Formal analysis, Visualization, Data curation. **M. El Ayoubi:** Writing – review & editing, Formal analysis, Data curation. **A. Samiri:** Writing – review & editing, Formal analysis, Data curation. **A. Atila:** Writing – review & editing, Conceptualization. **A. Hasnaoui:** Writing – review & editing, Visualization, Formal analysis, Data curation, Conceptualization, Supervision.

Declaration of competing interest

The authors declare that they have no known competing financial

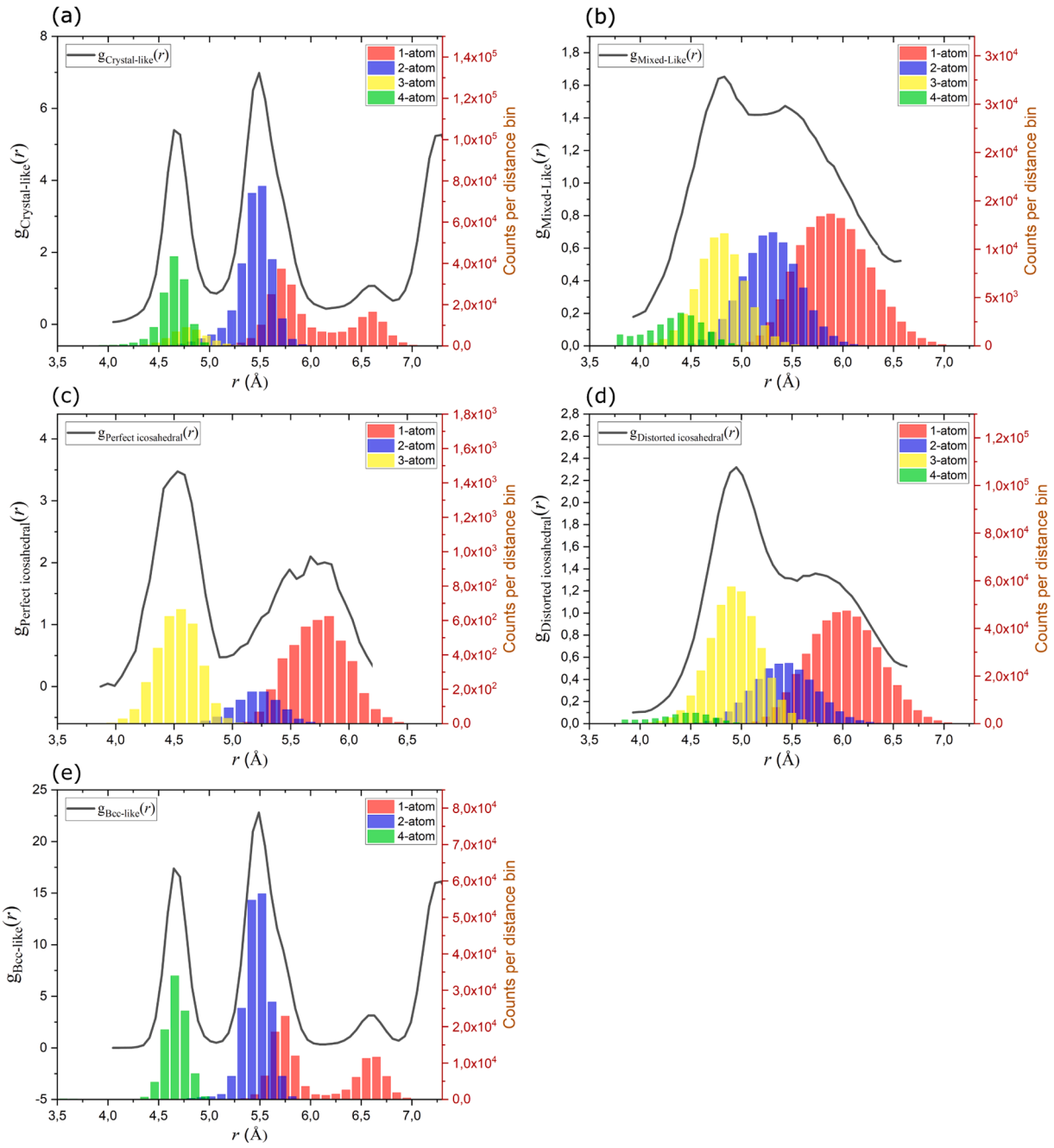

Fig. 10. Partial RDF curves of central atoms of (a) Crystal-like, (b) mixed-like, (c) perfect icosahedral, (d) distorted icosahedral and (e) bcc-like clusters in Ta at 300 K after quenching under 20 GPa.

interests or personal relationships that could have appeared to influence the work reported in this paper.

Data availability

Data will be made available on request.

References

[1] W. Klement, R.H. Willens, P. Duwez, Non-crystalline structure in solidified gold–silicon alloys, Nature 187 (1960) 869–870.
[2] A.L. Greer, Metallic glasses, Science 267 (1995) 1947–1953.
[3] H.F. Li, Y.F. Zheng, Recent advances in bulk metallic glasses for biomedical applications, Acta Biomater. 36 (2016) 1–20.
[4] A. Inoue, N. Nishiyama, New bulk metallic glasses for applications as magnetic-sensing, chemical, and structural materials, MRS Bull. 32 (2007) 651–658.
[5] M.M. Khan, A. Nemati, Z.U. Rahman, et al., Recent advancements in bulk metallic glasses and their applications: a review, Crit. Rev. Solid State Mater. Sci. 43 (2018) 233–268.
[6] D.B. Miracle, A structural model for metallic glasses, Nat. Mater. 3 (2004) 697–702.
[7] H.W. Sheng, W.K. Luo, F.M. Alamgir, et al., Atomic packing and short-to-medium-range order in metallic glasses, Nature 439 (2006) 419–425.
[8] X.J. Liu, Y. Xu, X. Hui, et al., Metallic liquids and glasses: atomic order and global packing, Phys. Rev. Lett. 105 (2010) 155501.
[9] S. Trady, M. Mazroui, A. Hasnaoui, et al., Molecular dynamics study of atomic-level structure in monatomic metallic glass, J. Non Cryst. Solids 443 (2016) 136–142.
[10] A. Khmich, K. Sbiaai, A. Hasnaoui, Annealing effect on elastic and structural behavior of Tantalum monatomic metallic glass, Mater. Chem. Phys. 243 (2020) 122636.
[11] X.J. Liu, Y. Xu, Z.P. Lu, et al., Atomic packing symmetry in the metallic liquid and glass states, Acta Mater. 59 (2011) 6480–6488.
[12] S.P. Pan, J.Y. Qin, W.M. Wang, et al., Origin of splitting of the second peak in the pair-distribution function for metallic glasses, Phys. Rev. B 84 (2011) 092201.

[13] P. Zhang, J.J. Maldonis, M.F. Besser, et al., Medium-range structure and glass forming ability in Zr–Cu–Al bulk metallic glasses, Acta Mater. 109 (2016) 103–114.
[14] S. Trady, A. Hasnaoui, M.M. hammed, et al., Local atomic structures of single-component metallic glasses, Eur. Phys. J. B 89 (2016) 223.
[15] M. Kbirou, S. Trady, A. Hasnaoui, et al., Cooling rate dependence and local structure in aluminum monatomic metallic glass, Philos. Mag. 97 (2017) 2753–2771.
[16] S. Trady, M. Mazroui, A. Hasnaoui, et al., Microstructural evolutions and fractal characteristics in medium range level in AlxNi100-x alloys during rapid solidification process, J. Alloys Compd. 744 (2018) 750–758.
[17] S. Abdelali, A. Khmich, A. Hassani, et al., Elastic and structural properties of Mg25Al75 binary metallic glass under different cooling conditions, J. Alloys Compd. 891 (2021) 161979.
[18] Y.-C. Liang, R.-S. Liu, Y.-F. Mo, et al., Influence of icosahedral order on the second peak splitting of pair distribution function for Mg70Zn30 metallic glass, J. Alloys Compd. 597 (2014) 269–274.
[19] M. Tahiri, A. Hassani, K. Sbiaai, et al., Investigating local atomic structural order in TiAl3 metallic glass using molecular dynamic simulation, Comput. Condens. Matter 14 (2018) 74–83.
[20] A. Khmich, K. Sbiaai, A. Hasnaoui, Structural behavior of tantalum monatomic metallic glass, J. Non Cryst. Solids 510 (2019) 81–92.
[21] S. Trady, A. Hasnaoui, M. Mazroui, Atomic packing and medium-range order in Ni3Al metallic glass, J. Non Cryst. Solids 468 (2017) 27–33.
[22] J. Ding, E. Ma, Computational modeling sheds light on structural evolution in metallic glasses and supercooled liquids, npj Comput. Mater. 3 (2017) 1–12.
[23] J. Ding, E. Ma, M. Asta, et al., Second-nearest-neighbor correlations from connection of atomic packing motifs in metallic glasses and liquids, Sci. Rep. 5 (2015) 17429.
[24] M. El Ayoubi, A. Khmich, A. Samiri, et al., Investigating medium range order in Mg-Al binary metallic glasses: molecular dynamics approach, J. Non Cryst. Solids 621 (2023) 122620.
[25] J. Mo, H. Liu, Y. Zhang, et al., Effects of pressure on structure and mechanical property in monatomic metallic glass, J. Non Cryst. Solids 464 (2017) 1–4.
[26] D. Jiang, D. Wen, Z. Tian, et al., Glass formation and cluster evolution in the rapidly solidified monatomic metallic liquid Ta under high pressure, Phys. A: Stat. Mech. Appl. 463 (2016) 174–181.
[27] A. Atila, M. Kbirou, S. Ouaskit, et al., On the presence of nanoscale heterogeneity in Al70Ni15Co15 metallic glass under pressure, J. Non Cryst. Solids 550 (2020) 120381.
[28] J. Jiang, W. Roseker, M. Sikorski, et al., Pressure effect of glass transition temperature in Zr46.8Ti8.2Cu7.5Ni10Be27.5 bulk metallic glass, Appl. Phys. Lett. 84 (2004) 1871–1873.
[29] J. Schroers, Glasses made from pure metals, Nature 512 (2014) 142–143.
[30] L. Zhong, J. Wang, H. Sheng, et al., Formation of monatomic metallic glasses through ultrafast liquid quenching, Nature 512 (2014) 177–180.
[31] S. Plimpton, Fast parallel algorithms for short-range molecular dynamics, J. Comput. Phys. 117 (1995) 1–19.
[32] R. Ravelo, T.C. Germann, O. Guerrero, et al., Shock-induced plasticity in tantalum single crystals: interatomic potentials and large-scale molecular-dynamics simulations, Phys. Rev. B 88 (2013) 134101.
[33] J.C. Zhang, C. Chen, Q.X. Pei, et al., Ab initio molecular dynamics study of the local atomic structures in monatomic metallic liquid and glass, Mater. Des. 77 (2015) 1–5.
[34] Y. Gan, Z. Sun, Y. Shen, Short-pulse laser formation of monatomic metallic glass in tantalum nanowire, Appl. Phys. A 123 (2016) 18.
[35] H. Liu, Z. Chen, J. Mo, et al., Brittle-to-ductile transition in monatomic tantalum nanoporous metallic glass, J. Non Cryst. Solids 506 (2019) 6–13.
[36] A. Stukowski, Visualization and analysis of atomistic simulation data with OVITO–the open visualization tool, Modell. Simul. Mater. Sci. Eng. 18 (2009) 015012.
[37] S. Sengul, M. Celtek, Pressure effects on the structural evolution of monatomic metallic liquid hafnium, Bitlis Eren Üniv. Fen Bilimleri Dergisi 7 (2018) 144–158.
[38] D. Jiang, D. Wen, Z. Tian, et al., Glass formation and cluster evolution in the rapidly solidified monatomic metallic liquid Ta under high pressure, Phys. A: Stat. Mech. Appl. 463 (2016) 174–181.
[39] G. Abrosimova, V. Chirkova, E. Pershina, et al., The effect of free volume on the crystallization of Al87Ni8Gd5 amorphous alloy, Metals (Basel) 12 (2022) 332.
[40] S. Abdelali, A. Khmich, H. Haouas, et al., Structural and mechanical behaviors of Mg-Al metallic glasses investigated by molecular dynamics simulations, Comput. Mater. Sci. 184 (2020) 109895.
[41] U. Domekeli, A molecular dynamic study of the effects of high pressure on the structure formation of liquid metallic Ti62Cu38 alloy during rapid solidification, Comput. Mater. Sci. 187 (2021) 110089.
[42] G. Guo, Quasi-icosahedral clusters in Zr-based metallic glasses, Metals (Basel) 10 (2020) 1135.
[43] J. Han, C. Wang, X. Liu, et al., Atomic-level mechanisms of nucleation of pure liquid metals during rapid cooling, ChemPhysChem 16 (2015) 3916–3927.
[44] F. Li, J. Zhang, X. Xu, et al., Influence from connection of atomic clusters on the second peak splitting of pair distribution function in metallic glasses, J. Non Cryst. Solids 600 (2023) 122021.
[45] Z.-Y. Hou, L.-X. Liu, R.-S. Liu, et al., Short-range and medium-range order in Ca7Mg3 metallic glass, J. Appl. Phys. 107 (2010) 083511.
[46] M. Lee, C.-M. Lee, K.-R. Lee, et al., Networked interpenetrating connections of icosahedra: effects on shear transformations in metallic glass, Acta Mater. 59 (2011) 159–170.